RSC Advances

PAPER

View Article Online
View Journal | View Issue

Cite this: *RSC Adv.*, 2020, **10**, 31575

Study on photovoltaic stability and performance by incorporating tetrabutyl phosphonium iodide into the active layer of a perovskite type photovoltaic cell

Edgar González-Juárez,[a] Karen Valadez-Villalobos,[a] Diana F. Garcia-Gutierrez,[b] Domingo I. Garcia-Gutierrez,[b] Arian Espinosa Roa[c] and Eduardo Sanchez[*a]

Received 25th May 2020
Accepted 11th August 2020

DOI: 10.1039/d0ra04630b

rsc.li/rsc-advances

A simple synthesis of an ionic liquid is carried out using a trialkylphosphine and an alkyl halide. The results showed that the quality of perovskite crystals is enhanced by the incorporation of B_4PI, when the percentage is 1.5% the PCE of champion PSCs $MA_{98.5}(B_4PI)_{1.5}PbI_3$ increases significantly from 15.5%, with a V_{OC} of 0.957 mV, J_{SC} of 23.6 mA cm^{-2}, and an FF of 68.4%. Stability tests show that excess B_4PI by 20% has a protective effect against humidity, $MA_{80}(B_4PI)_{20}PbI_3$ was more stable towards humidity, losing only 20% efficiency for 200 h.

1. Introduction

In the past decade, perovskite solar cells (PSCs) have attracted extensive research interest due to their simple preparation method,[1] adjustable band gap,[2–4] high performance, large absorption coefficient,[5,6] light weight, long carrier diffusing distance and solution processability.[7,8] The highest certified power conversion efficiency (PCE) reported for PSCs has reached 25.2% based on a simple solution process.[9] One of the keys to success for PCE high performance, has been optimizing the quality of $MAPbI_3$ films, in fact, the performance of the solar cell is influenced significantly by both morphology and crystallinity of the film, which are formed through the crystallization process of perovskite materials. There is a series of thermodynamic and kinetic steps (deposition of atoms, diffusion, nucleation, and growth) in the crystallization process. These steps may be influenced by moisture differently and understanding them can help to improve the quality of the final films.[10] In this sense, different strategies have been developed to enhance the PSCs efficiency by controlling the quality of the perovskite thin film, such as sequential and one-step deposition, vacuum deposition, and vapor assisted solution processing.[11–14]

Conventional perovskite materials (such as $MAPbX_3$ and $FAPbX_3$, MA = CH_3NH_3, FA = $CH(NH_2)_2$, X = Cl, Br, or I) usually suffer from the problem of low environmental stability.[15] Factors such as humidity, heat and, sun light irradiation significantly affect the performance and stability of PSCs.[16,17] The moisture instability might be overcome, in part by molecular engineering or encapsulation with hydrophobic layers.[18] Recently, alternative two-dimensional (2D) halide perovskites have quickly become a promising alternative to three-dimensional (3D) perovskite solar cell absorbers, and in other applications, such as light emitting diodes,[19] phosphors,[20] transistors,[21] photodetectors[22] and lasers.[23] However, 2D perovskites with rigid crystalline structures have a wide range of energy band gap, which limits their application in photovoltaic devices.[24] Therefore, 3D/2D perovskite dimensional combination could improve stability by the presence of hydrophobic cations that promote chemical and thermal stability, in addition to having the option of different organic cations, while the 3D structure could improve charge carrier transfer processes.[25] Among the different organic cations recently explored, ionic liquids (IL) have been studied due to their interesting properties, such as good solubility, wide temperature range in the liquid state, good thermal stability, as well as low toxicity that can be applied in the manufacture of photovoltaic devices.[26] Phosphonium salts have been reported alternative IL for solar cells applications, for example, Ma *et al.*, (2020)[27] used phosphonium halides salts substituted with aromatic groups and carbazole as passivating agents on the surface of $MAPbI_3$. The passive layer managed to suppress recombination at the interface between the HTM and the perovskite. Garcia Gutierrez *et al.*, (2018),[28] performed the synthesis of different tetra-alkylphosphonium derivatives with different numbers of

---

[a] *Universidad Autónoma de Nuevo León, UANL, Facultad de Ciencias Químicas, FCQ, Av. Universidad s/n, Cd. Universitaria, San Nicolás de los Garza, Nuevo León, C. P. 66450, Mexico. E-mail: eduardo.sanchezcv@uanl.edu.mx*

[b] *Universidad Autónoma de Nuevo León, UANL, Facultad de Ingeniería Mecánica y Eléctrica, FIME, Av. Universidad s/n, Cd. Universitaria, San Nicolás de los Garza, Nuevo León, C. P. 66450, Mexico*

[c] *CONACyT-Centro de Investigación en Química Aplicada, Unidad Monterrey, Parque de Innovación e Investigación Tecnológica (PIIT), Alianza Sur, No. 204, C. P. 66628, Apodaca, Nuevo León, Mexico*

carbons in the alkyl chain, R = ethyl, butyl, hexyl, and octyl, to form perovskite-like hybrid compounds with BiI_3. The compounds $(R_4P)_xBi_yI_z$ displayed good humidity stability (40%) for 3000 h, and are good candidates for testing on photovoltaic devices. Grätzel *et al.*, (2015)[29] managed to modify the surface of $MAPbI_3$ by adding 4-amino butylphosphonic acid chloride, which acted as a crosslinker between perovskite grains through the strong interaction between the $PO(OH)_2$ and NH_3^+ terminal groups and the perovskite surface.

Despite the fact that most of its applications are focused on the area of catalysis, phase transfer reactions and extraction processes,[30] phosphonium halides salts have important properties that can be applied to photovoltaic devices and represent an alternative to replace other ILs such as those derived from imidazolium salts. Phosphonium halides possess similar electronic characteristics to ammonium halides, which have rarely been investigated for surface passivation of PSCs.[27]

On the other hand, the methods of synthesis of alkylphosphonium salts are relatively simple, generating compounds with different alkyl or aryl groups which play an important role in fine-tuning their properties. Based on this background and to the low application of phosphonium salts in the photovoltaic area, in this research project an alkylphosphonium functionalized with four alkyl chains (B_4PI) was synthesized, with the aim of studying the effect it generates on the property structure of $MAPbI_3$ when incorporated in different percentages by weight.

2. Experimental

2.1. Materials

All the chemicals were used as received, including titanium diisopropoxide bis(acetylacetonate) (75 wt% in isopropanol, Sigma-Aldrich), 1-butanol (99.8%, Sigma-Aldrich), titanium dioxide (TiO_2) paste (Dyesol 18NR-T), PbI_2 (99.9983%,Sigma-Aldrich), *N*,*N*-dimethylformamide (DMF, anhydrous 99.5%, Sigma-Aldrich), lithium bis(trifluoromethylsulfonyl)imide (Li-TFSI, Sigma-Aldrich), spiro-MeOTAD (99%, Shenzhen Feiming), chlorobenzene (SigmaAldrich), acetone, ethanol and, acetonitrile. The morphological characteristics of the thin films were observed by scanning electron microscopy (SEM) in a JEOL JCM-6000 and a Hitachi SU-8020. X-ray diffraction (XRD) was employed to characterize the crystallinity of the films using an XRD Bruker D2 phaser. The UV-Vis transmission spectra were characterized by using a scientific evolution 300 spectrometer. NMR spectroscopy (Bruker Avance III of 500 MHz). The 1H chemical shifts (δ) are reported in ppm. The spectra were obtained at 500 MHz in $CDCl_3$.

2.2. Perovskite standard solar cell device construction

Fluorine doped tin oxide (FTO) glass was patterned by chemical etching with zinc (Zn) powder and chloride acid (HCl) solution. The etched substrate was then cleaned with hellamanex 2% and ultrasonically cleaned with 2-propanol and deionized water in sequence for 15 min, respectively. Afterward, the substrates were further cleaned using O_2 plasma cleaning for 15 min. A dense layer of TiO_2 was then coated on the substrates by spin coating of titanium diisopropoxide bis(acetylacetone) (75 wt% in isopropanol, Aldrich) diluted in absolute ethanol (v/v, 1/20) at 3000 rpm for 1 min. The substrates were then heated at 180 °C for 5 min followed by annealing at 450 °C for 1 h. A mesoporous layer of TiO_2 was then deposited by spin-coating TiO_2 paste (Dyesol 18NR-T) diluted in absolute ethanol at 1 : 12 weight ratio at 5000 rpm for 30 s. The substrates were then heated at 180 °C for 5 min, followed by annealing at 450 °C for 1 h. For the fabrication of the standard cell, the methodology proposed by Sutanto *et al.*, 2017,[31] was followed, using DMF as solvent. Previously prepared solution 1.25 M of PbI_2 : MAI with a 1 : 1 molar ratio and left at 70 °C for 12 h. $MAPbI_3$ solution was deposited by spin-coating on the mesoporous layer of TiO_2 at 3000 rpm for 30 s. After 6 s of having started the centrifugation technique, 650 μL of chlorobenzene were rapidly added to the substrate. Furthermore, a hole transport material (HTM) of spiro-OMeTAD was spin-coated at 3000 rpm for 30 s from a chlorobenzene solution (79.1 mg in 690 μL) that contained 22 μL of 4-*tert*-butylpiridine and 15 μL of Li-TFSI (bis(trifluoromethane)sulfonimide lithium salt) from a 500 mg mL^{-1} stock solution in acetonitrile as dopants (Fig. 1).

To study the effect of B_4PI on $MAPbI_3$, and on the performance of the photovoltaic device, B_4PI was incorporated in different percentages by weight (% w/w) (Table 1). The perovskite film was deposited also by spin coating a previously prepared solution 1.25 M of MAI : PbI_2 with a 1 : 1 molar relation in a solvent mixture of DMF/DMSO (80 : 20 v/v) by a one-step process at 5000 rpm for 30 s. After a 6 s delay time of the spin coating process, a 650 μL of anhydrous chlorobenzene were added on top of the substrate. Additionally, perovskite thin films were sintered at 100 °C for 10 min. HTM (hold transport material, spiro-OMeTAD) was spin coated at 3000 rpm for 30 s. Finally, an 80 nm thick silver counter electrode was deposited under high vacuum by physical vapor deposition.

2.3. Photovoltaic characterization

The *J*–*V* curves were measured using a solar simulator (Newport, Oriel Instruments, 91160A) with a source meter (Keithley 2400). In addition, a xenon lamp was used as a light source and it was calibrated using a silicon reference solar cell (enlitech) to regulate the output power of the lamp to 1000 W m^{-2}.

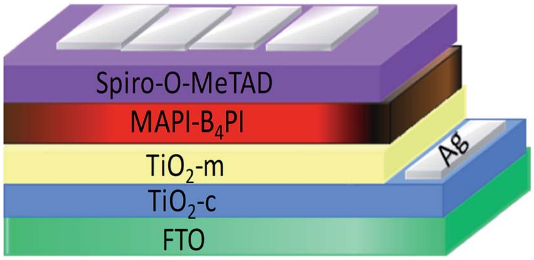

Fig. 1 Configuration of the cell based on the modified perovskite layer.

Table 1 Different compositions (w/w%) utilized in the synthesis of derivatives solutions $MAPbI_3$-B_4PI

Solution	PbI_2 (mg)	$CH_3CH_2NH_3I$ (mg)	B_4PI (mg)
$MAPbI_3$	289	100	0
$MA_{98.5}(B_4PI)_{1.5}PbI_3$	289	98.5	1.5
$MA_{97}(B_4PI)_3PbI_3$	289	97	3
$MA_{95}(B_4PI)_5PbI_3$	289	95	5
$MA_{90}(B_4PI)_{10}PbI_3$	289	90	10
$MA_{80}(B_4PI)_{20}PbI_3$	289	80	20
B_4PI	0	0	5

The measurements were performed inside the glove box in order to protect the stability of the cells. The cell area was limited using a metal mask (0.254 cm × 0.254 cm). The active area of device is 0.065 cm^2.

2.4. Synthesis tetrabutyl fosfonio iodide (B_4PI)

The synthesis was carried out inside a glove dry box with a N_2 atmosphere due to the reactivity of tributyl phosphonium (B_3P). In an amber bottle, 2.667 g of butyl iodide (BI) were weighed and mixed with 3.0108 g of B_3P in a 1 : 1 stoichiometric ratio. The mixture was sonicated for 18 h outside the dry chamber (Fig. 2). NMR ($CDCl_3$) ^1H (500 MHz): δ(ppm) = 0.96 (t 3H); 1.55 (m, 2H); 0.96(t, J = 3H); 1.70 (m, 2H); 2.54 (m, 2H); 31P: δ(ppm) = 32.8 (s).

3. Results

3.1. Purification and incorporation B_4PI on $MAPbI_3$

The synthesis of phosphonium salts are S_N2-type reactions and have been extensively studied. Some methodologies show long synthesis times and generation of secondary products or impurities.[32,33] In our case, the synthesis of B_4PI was carried out using the methodology proposed by Varma *et al.*, 2002,[34] which consists of carrying out the synthesis by ultrasound assistance. Under this methodology it is possible to reduce reaction times and generation of impurities. B_4PI was obtained as a bright white solid and was washed several times with petroleum ether to purify it. For this, 15 mL of petroleum ether were added and further sonicated. The purification was monitored by UV-vis spectrophotometry in transmittance mode. Fig. 3a shows the progress during B_4PI purification, the petroleum ether carries impurities in each of the washes, at the end B_4PI spectrum is very similar to the solvent spectrum. In this moment the analysis was suspended. Finally, B_4PI was subsequently dried in a vacuum oven overnight.

FT-IR analysis of B_4PI and its precursors show very similar signals due to the similarity of the functional groups, however, some differences allow us to establish the obtaining of B_4PI, such as the signal corresponding to the C–I covalent bond of the alkyl halide (BI) disappears in B_4PI due to the ionic nature of the salt. On the other hand, there are changes in intensity of the signals when incorporating the alkyl chain, for example the signals that appear in 3000–2850 and 1300 corresponding to the alkyl groups ($-CH_3$ and $-CH_2$), the same occurs for the corresponding bands of $P-CH_2$ at 1400 cm^{-1} (Fig. 3b). Table 2 summarizes the absorption bands for each of the compounds.

On the other hand, ^1H, ^{31}P NMR characterization techniques were employed to ensure B_4PI purification (Fig. 3c; 3d) respectively. The ^1H NMR spectrum shows at high field the characteristic chemical shifts of protons associated with the alkyl chains at δ = 0.96 to 2.54 ppm. While the ^{31}P NMR spectrum contains a single signal at δ = 32.7 ppm, indicating a complete transformation of triphenylphosphine.

3.2. Perovskite film fabrication strategies and DRX, SEM analysis

Once B_4PI was characterized and purified, it was added to the perovskite precursor solution to analyze its effect on a thin layer and the efficiency of a perovskite solar cell of $MAPbI_3$. B_4PI, was added in different percentages by weight, as indicated in the experimental section. Furthermore, two reference targets (100% $MAPbI_3$ and 100% B_4PI) were prepared in order to compare and better understand composition variations. It is important to comment that solvent engineering plays a very important role in the quality of the films. In this work, a mixture of DMF : DMSO solvents was used in a 4 : 1 ratio to promote the formation of the MAI-PbI_2-DMF and MAI-PbI_2-DMSO adducts that delay perovskite crystallization. Dimethylformamide (DMF), dimethylsulfoxide (DMSO) and γ-butyrolactone (GBL) are most widely used solvents for perovskite preparation due to the high boiling point and low vapor pressure.[35–37] On the other hand, it is well known that the incorporation of co-solvents by the deposition technique dynamically contributes to generate a dense and uniform layer. In this case, chlorobenzene was used and deposited 6

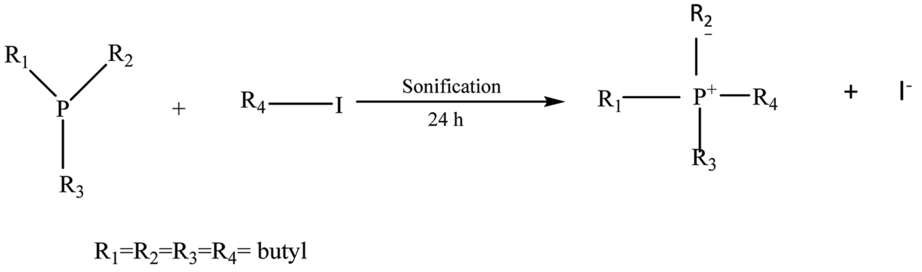

Fig. 2 Reaction scheme for B_4PI synthesis.

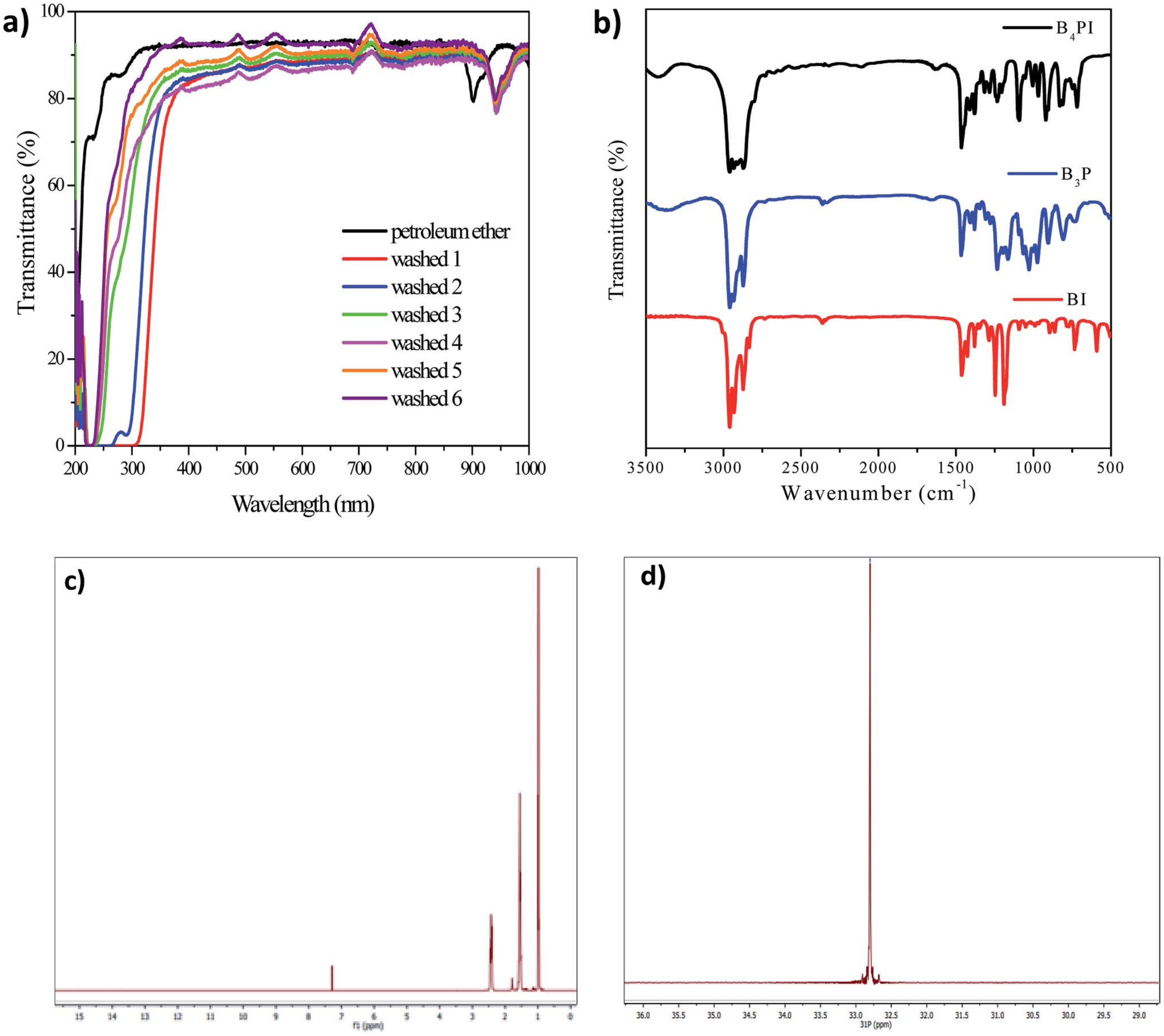

Fig. 3 Purification and characterization of B_4PI; (a) UV-vis spectra in mode transmittance, (b) FT-IR analysis, (c) RMN analysis ^1H; (d) ^{31}P.

seconds after starting the spinner. Finally, the films were subjected to a heat treatment of 100 °C for 10 minutes (Fig. 4).

The addition of B_4PI in different percentages and the use of the solvent-engineering process significantly improved the quality of the films. The analysis by scanning electron microscopic (SEM) show the morphology of pristine $MAPbI_3$, $MA_{98.5}(B_4PI)_{1.5}PbI_3$ and $MA_{80}(B_4PI)_{20}PbI_3$, films of lower and higher concentration of B_4PI, respectively (Fig. 5).

The pristine $MAPbI_{3,}$ film showed a random grain size distribution. While this grain size increased when B_4PI was incorporated into the perovskite precursor solution. $MA_{98.5}(B_4PI)_{1.5}PbI_3$ showed a larger grain size and no clear defects in its morphology, while $MA_{80}(B_4PI)_{20}PbI_3$, with a higher B_4PI concentration, showed a larger crystal grain size, but with the presence of defects, such as pin-holes.

On the other hand, X-ray diffraction (XRD) is one of the most specific techniques for the qualitative and quantitative analysis of crystalline phases of any type of material. Numerous studies

Table 2 IR absorption bands (cm^{-1}) and their assignments for B_4PI

Assignment	BI	B_3P	B_4PI
ν C–H$_{\text{stretching}}$	3056	3056	3041
ν C–H	2875	2878	2853
ν CH_3 $_{\text{symmetric}}$	1377	1376	1375
ν CH_3 $_{\text{asymmtric}}$	1460	1457	1467
ν $(CH_2)_n$ $_{\text{rock}}$	788	807	819
ν C–I	650	—	—
ν C–P	—	1045	1086
ν P–CH_2	—	1467	1477

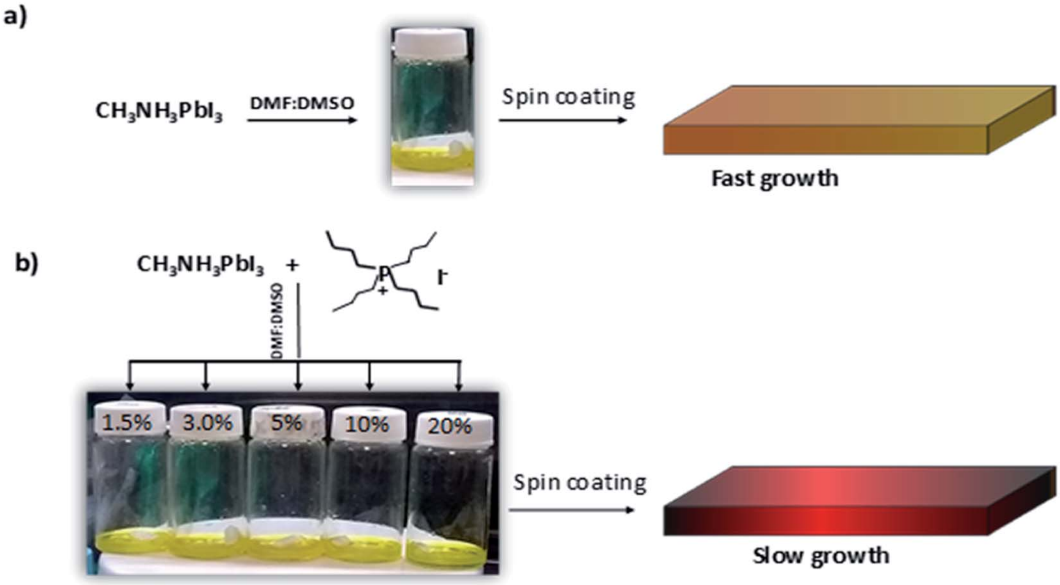

Fig. 4 Strategy and preparation of films derived from $MAPbI_3$-B_4PI; (a) pristine $MAPbI_3$; (b) $MAPbI_3$ with the alkylphosphonium additives.

show the importance of using this technique to identify the formation of new phases when a cation is incorporated into another system. In this sense, the $MAPbI_3$, B_4PI films and the different $MAPbI_3:B_4PI$ mixtures were analyzed by XRD to identify the possible formation of a new phases derived from B_4PI. First, Fig. 6a shows the diffractograms of each of the variables and shows the characteristic $MAPbI_3$ pattern observed at 14.1°, 20°, 23.5°, 24.5°, 28.5°, 31.9°, 40.6°, and 43.2° that correspond to the planes (1 1 0), (1 1 2), (2 1 1), (2 0 2), (2 2 0), (3 1 0), (2 2 4), (3 1 4), respectively. In addition, the diffractograms show an increase in the intensity of the peaks when B_4PI is added in each of the thin layers, this is an indication that B_4PI improves the crystallinity of perovskite. On the other hand, it has been reported that the modification of long chain organic molecules within 3D perovskites can promote the formation of 2D layer structures,[38,39] improving thermal and humidity stability.[40] Based on this discussion, the 2D perovskite B_4PIPbI_3 was synthesized from the precursors PbI_2 and B_4PI, in order to compare the diffractograms in the region below $2\theta = 10°$. The comparative analysis shows that the diffractograms of the $MA_{80}(B_4PI)_{20}PbI_3$ and $MA_{90}(B_4PI)_{10}PbI_3$ films show a peak at $2\theta = 7.2°$, which correlates with the peak of the 2D perovskite (Fig. 6b).[41] On the other hand, the $MA_{95}(B_4PI)_5PbI_3$ and $MA_{97}(B_4PI)_3$ PbI_3 films also showed also a peak at $2\theta = 9°$. This proves that the addition of B_4PI in different percentages by weight determine the properties and effects on each film. Therefore, this effect will be analyzed and discussed and in the following section.

3.3. Thin film stability tests

Stability tests were performed in a room with 30% controlled relative humidity (RH). The analysis was carried out in a thin film and was monitored by XRD at different times. It has been reported that prolonged exposure to moist air will degrade a methylammonium lead iodide perovskite film.[42] The degradation mechanism has been extensively studied and as a result

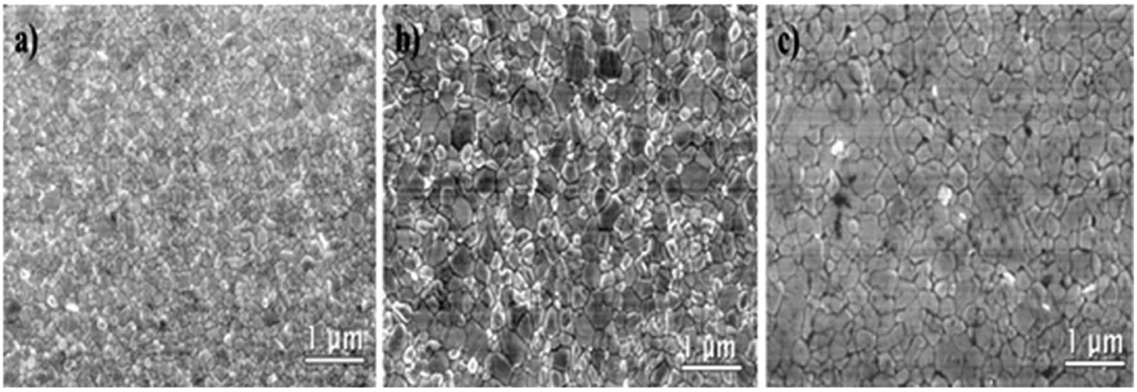

Fig. 5 Scanning Electron Microscopy (SEM) images for the $MAPbI_3$ perovskite layers; (a) $MAPbI_3$, (b) $MA_{98.5}(B_4PI)_{1.5}PbI_3$, (c) $MA_{80}(B_4PI)_{20}PbI_3$.

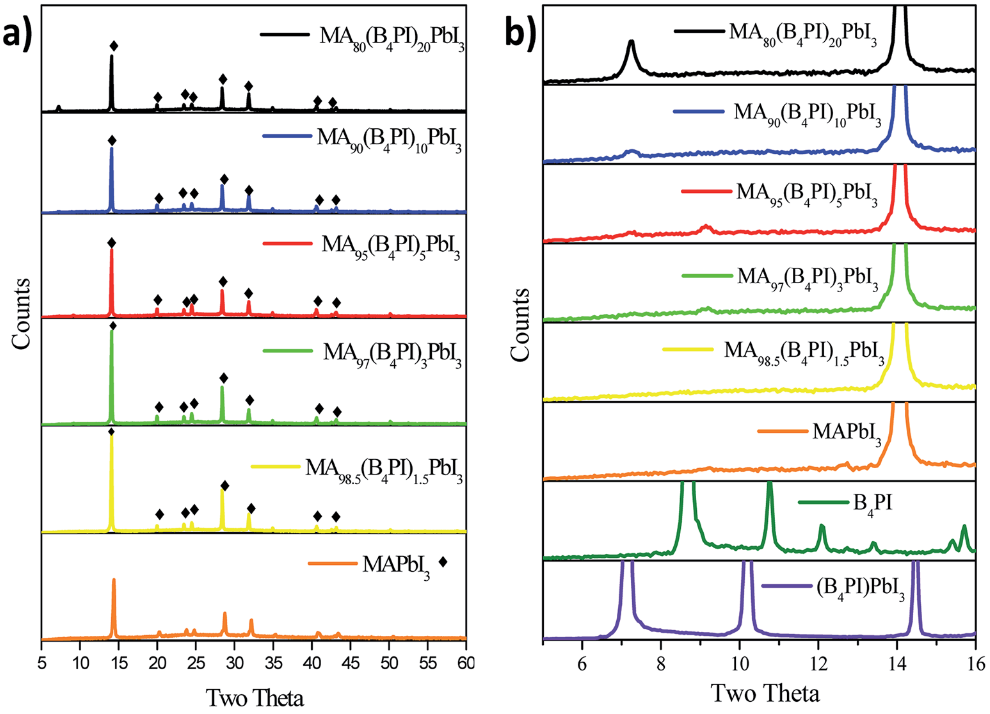

Fig. 6 (a) XRD patterns of pristine $MAPbI_3$ and $MA_{1-x}(B_4PI)_xPbI_3$ films; (b) highlighted diffraction profiles in the range from $2\theta = 10°–16°$.

of material degradation the by-products generated are hydroiodic acid (HI), solid lead iodide (PbI_2) and methylammonium cations (MA^+) released as gas (amine) or dissolved in water.[43] The diffractograms show the evolution of the degradation of each film (Fig. 7). At the beginning of the analysis, the presence of the characteristic peak of $PbI_2 = 12.5°$ is not observed. However, as the exposure time increases, the peak starts to appear. Table 3 shows the times when the degradation started. $MAPbI_3$ started the degradation process at 48 h, while the films with B_4PI began to degrade at longer times. The incorporation of B_4PI has a positive effect against the degradation of $MAPbI_3$, as can be seen in Table 3. In addition, it is well known that IL can diffuse as tunneling layers and act as encapsulation layers to protect films from decomposition caused by moisture.[44]

The results show that the incorporation of 1.5% of B_4PI was the best percentage to improve the stability and photovoltaic performance of $MAPbI_3$. In this percentage the perovskite stability is improved by the interaction between the free electron pairs of phosphorus and Pb^{2+}, in addition, hydrophobic alkyl chains promote the formation of a more homogeneous film that improves crystallinity and grain size, improving stability and photovoltaic performance. These results are agreement with those made by Wu *et al.*, (2020)[45] when they added a symmetric tetrabutylammonium salt to perovskite. In relation to this topic, Liu *et al.* (2017)[46] introduced the ionic liquid, methyltrioctylammonium trifluoromethanesulfonate (MATS) to passivate the traps and grain boundaries near the perovskite top surface, they comments that the ionic interactions between the $CF_3SO_3^-$ anion (or $[CH_3(CH_2)_6CH_2]_3CH_3N^+$ cation) of MATS and MA^+ cation (or $[PbI_6]_4^-$) in the perovskite crystal lattice ensure its excellent affinity to the perovskite surface. On the other hand, it was observed that by increasing the percentage of B_4PI less homogeneous films were generated, with surface defects that cause faster degradation such as its observed in the micrographic. However, the stability tests on the photovoltaic devices had a different behavior.

B_4PI incorporation was analyzed in thin layer by UV-vis and PL. In general, the absorption spectra show an onset at 760 nm can be observed in each of the samples (Fig. 8a). However, for $MA_{80}(B_4PI)_{20}PbI_3$ showed a slight blue shift, which agrees with the emission spectrum. According to other studies, this displacement is associated with the presence of 2D-3D perovskite in the film[47,48] which is confirmed by the XRD analysis. Even so, problems associated with the quality of the perovskite film showed less intensity in PL (Fig. 8b). In contrast, $MA_{98.5}(B_4PI)_{1.5}PbI_3$ presented high intensity, which suggests the passivation of the trap states on the surface that prevents the recombination of charges, in fact the efficiency achieved was the highest of all the devices evaluated.

Fig. 9a shows the *J*–*V* curves for the devices fabricated and Table 4 shows their photovoltaic parameters. The PCE for pristine perovskite solar cell is 14%, with open circuit voltage (V_{OC}) of 947 mV, a short circuit current density (J_{SC}) of 22.6 mA cm^{-2} and a fill factor (FF) of 64.6%. The cell that presented the best efficiency was the one fabricated with thin film $MA_{98.5}(B_4PI)_{1.5}PbI_3$, meaning, when B_4PI was added at 1.5%, with a photovoltaic yield of 15.5%, with a (V_{OC}) of 957.4 mV, (J_{SC}) of 23,6 mA cm^{-2} and (FF) of 68.4%. This improvement is attributed to the formation of high-quality perovskite grains by addition of B_4PI. However, when increasing the percentage of B_4PI, the effect was not as significant, for example the efficiency of $MA_{80}(B_4PI)_{20}PbI_3$ was only 10% with a (V_{OC}) = 963 mV,

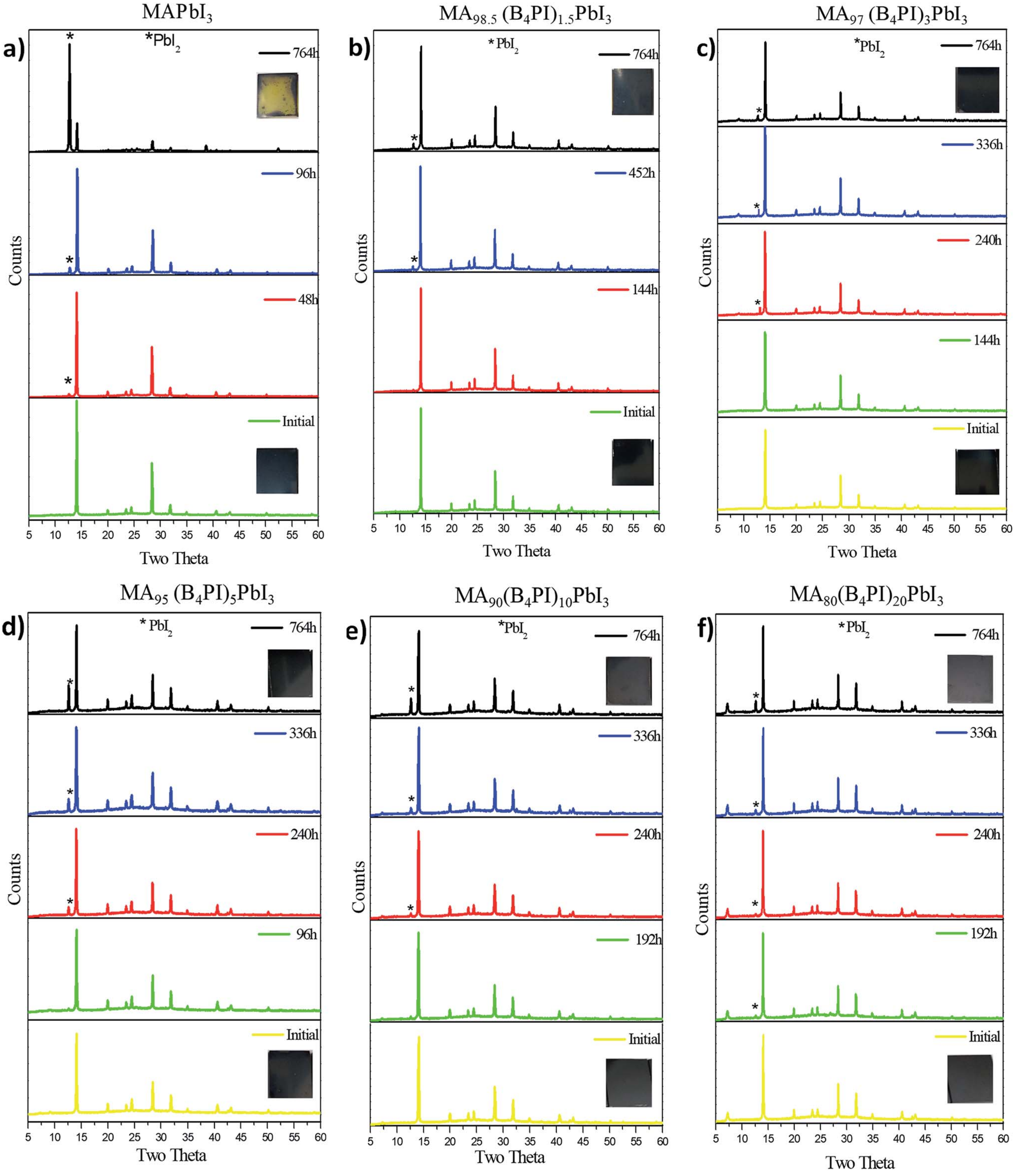

Fig. 7 XRD of film degradation: (a) pristine $MAPbI_3$; (b–f) $MA_{1-x}(B_4PI)_xPbI_3$.

a decrease in (J_{SC}) = 20.16 mA cm^{-2} and an (FF) = 51.1%. This result is also attributed to the quality of the film, as it was seen on the SEM analysis, thin film showed the presence of pin-holes in its morphology. It is well known that the presence of traps in films generate the recombination of the exciton generator in the active layer of the cell.

Photovoltaic devices were subjected to stability tests under the same conditions used for the thin films. As expected, pristine $MAPbI_3$ quickly loses 50% of its PCE within the first 24 h; on the other hand, $MA_{98.5}(B_4PI)_{1.5}PbI_3$ loses half of its PCE after 200 h. It is important to note that $MA_{80}(B_4PI)_{20}PbI_3$ presented the lowest efficiency (10%), however, in the stability tests it only

Table 3 Onset of film degradation

Thin film	Onset (h)
$MAPbI_3$	48
$MA_{98.5}$ $(B_4PI)_{1.5}PbI_3$	452
$MA_{97}(B_4PI)_3PbI_3$	240
$MA_{95}(B_4PI)_5PbI_3$	240
$MA_{90}(B_4PI)_{10}PbI_3$	240
$MA_{80}(B_4PI)_{20}PbI_3$	192

lost 20% of its PCE in the same time span studied (Fig. 9b). In this case, we should notice that the timescales of degradation of films *versus* time degradation of devices is remarkably different, the device lifetime is affected by additional stressors related to working conditions of a cell. However, we have also associated that the stability in the photovoltaic performance of $MA_{80}(B_4PI)PbI_3$ is due, to the formation of a new phase of 2D perovskite that acts as a passive layer in the $MAPbI_3$ film, the deposition of a bulky organic cation on a pre-formed 3D perovskite surface induces *in situ* growth of a 2D perovskite layer through a reaction with excess PbI_2. This approach improves the stability and photovoltaic performance due to the decreased number of surface trap states and suppressed interfacial charge recombination by the favorable band alignment of the 3D/2D mixed-layered structure.[44] Another possible reason is that B_4PI acts as a Lewis base to coordinate Pb ions by donating electronic

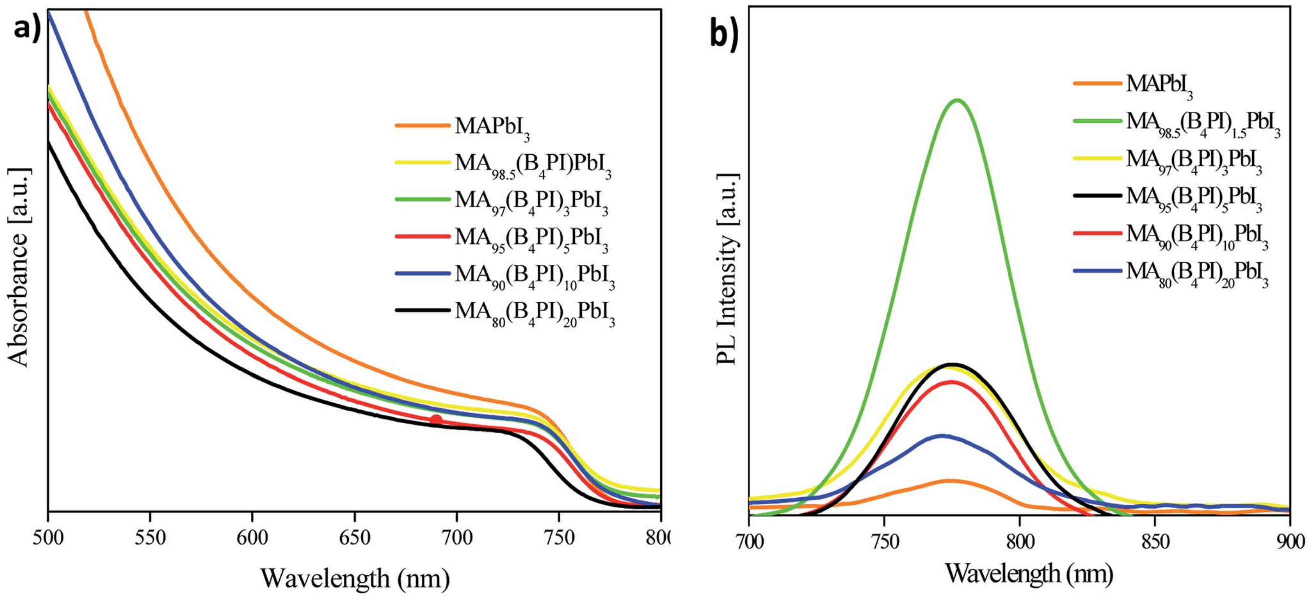

Fig. 8 Spectroscopic studies of perovskite films (a) absorption spectra; (b) PL spectra.

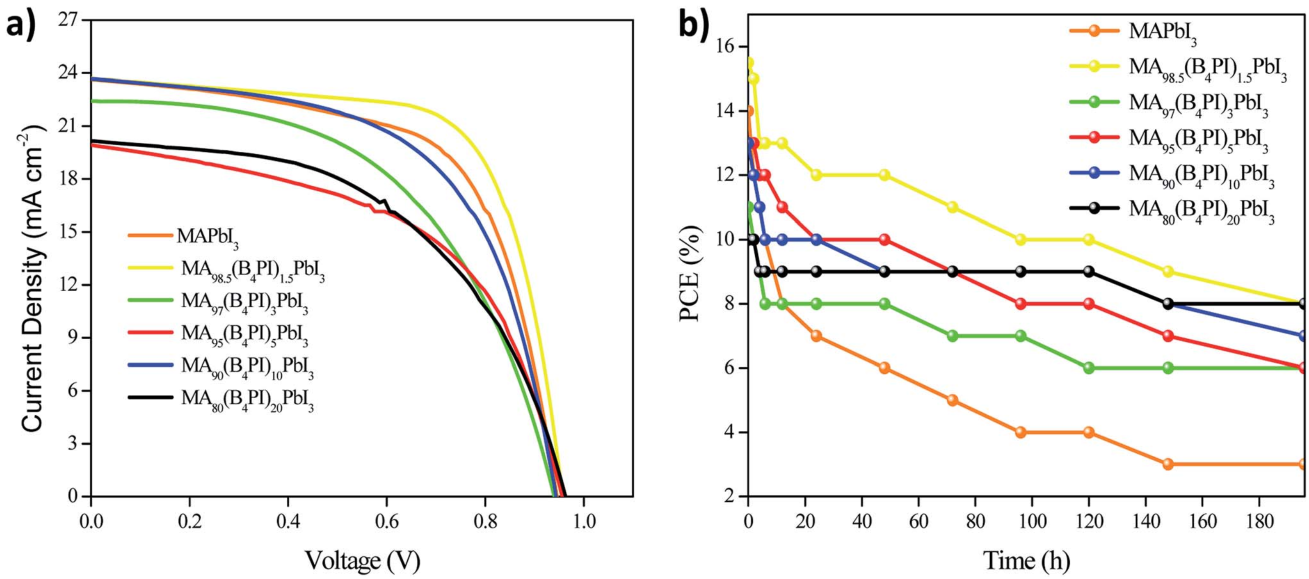

Fig. 9 (a) *J–V* curves of the best performing devices; (b) stability of photovoltaics devices.

Table 4 Photovoltaic parameters of fabricated devices

Photovoltaic device	V_{OC} (mV)	J_{SC} (mA cm^{-2})	FF (%)	Eff. (%)
$MAPbI_3$	945.7	22.6	64.6	14
$MA_{98.5}(B_4PI)_{1.5}PbI_3$	957.4	23.6	68.4	15.5
$MA_{97}(B_4PI_3)_3PbI_3$	940.3	22.4	52.3	11
$MA_{95}(B_4PI)_5PbI_3$	956.2	19.9	53.2	10.1
$MA_{90}(B_4PI)_{10}PbI_3$	943.9	23.68	58.5	13
$MA_{80}(B_4PI)_{20}PbI_3$	963.3	20.16	51.5	10

density to passivate traps at the interface between perovskite and spiro-OMeTAD and at the same time the hydrophobic character of the alkyl chains protect from moisture, resulting in the stability of the device. Different investigations show the same results when incorporating Lewis bases as derivatives of alkylthiophenes and pyridine.[49,50]

4. Conclusions

In conclusion, a simple synthesis of an ionic liquid was carried out using a trialkylphosphine and an alkyl halide. The results showed that the quality of perovskite crystals is enhanced by the incorporation of B_4PI, particularly when the percentage added was 1.5%. The PCE of champion PSC featuring the thin films of $MA_{98.5}(B_4PI)_{1.5}PbI_3$, increases significantly to 15.5%, with a V_{OC}, J_{SC} and FF of 0.957 mV, 3.6 mA cm^{-2}, and 68.4%, respectively. This result in photovoltaic devices is attributed to the quality of the film and the intrinsic hydrophobicity of long B_4PI chains and the highly oriented density nature of the perovskite films, which prevents direct contact of water molecules. Lower efficiencies were achieved when the percentage was increased, however, stability tests on photovoltaic devices showed that when B_4PI is incorporated at 20%, the cell $MA_{80}(B_4PI)_{20}PbI_3$ retains 80% of its efficiency and is attributed to the formation of a 2D perovskite that passivates the perovskite surface and prevents recombination of the charges generated when subjected to solar radiation. In addition, B_4PI confers electron density on Pb ions to passivate traps at the perovskite interface and the hole transporting material.

Conflicts of interest

There are no conflicts to declare.

Acknowledgements

The authors would like to thank the Universidad Autónoma de Nuevo León, SENER-CONACyT for financially supporting this research under research project 256766 and project CONACyT FC-2015-2-1252.

References

1 F. X. Xie, C. C. Chen, Y. Z. Wu, X. Li, M. Cai, X. Liu, X. Yang and L. Han, Vertical recrystallization for highly efficient and stable formamidinium-based inverted-structure perovskite solar cells, *Energy Environ. Sci.*, 2017, **10**, 1942–1949.

2 I. Zimmermann, S. Aghazada and M. K. Nazeeruddin, Lead and HTM Free Stable Two-Dimensional Tin Perovskites with Suitable Band Gap for Solar Cell Applications, *Angew. Chem., Int. Ed.*, 2019, **58**, 1072–1076.

3 Y.-N. Zhang, B. Li, L. Fu, Y. Zou, Q. Li and W. L. Yin, Enhanced optical absorption and efficient cascade electron extraction based on energy band alignment double absorbers perovskite solar cells, *Sol. Energy Mater. Sol. Cells*, 2019, **194**, 168–176.

4 D. Zhao, C. Chen, C. Wang, M. M. Junda, Z. Song, C. R. Grice, Y. Yu, C. W. Li, B. Subedi, N. J. Podraza, X. Z. Zhao, G. Fang, R.-G. Xiong, K. Zhu and Y. F. Yan, Efficient two-terminal all-perovskite tandem solar cells enabled by high-quality low-bandgap absorber layers, *Nat. Energy*, 2018, **3**, 1093–1100.

5 D. P. Mcmeekin, G. Sadoughi, W. Rehman, G. E. Eperon, M. Saliba, M. T. Hörantner, A. Haghighirad, N. Sakai, L. Korte, B. Rech, M. B. Johnston, L. M. Herz and H. J. Snaith, A mixed-cation lead mixed-halide perovskite absorber for tandem solar cells, *Science*, 2016, **351**, 151–155.

6 T. W. Ng, H. T. Chandran, C. Y. Chan, M. F. Lo and C. S. Lee, Ionic Charge Transfer Complex Induced Visible Light Harvesting and Photocharge Generation in Perovskite, *ACS Appl. Mater. Interfaces*, 2015, **7**, 20280–20284.

7 W. S. Yang, J. H. Noh, N. J. Jeon, Y. C. Kim, S. Ryu, J. Seo and S. I. Seok, Solar Cells. High-performance photovoltaic perovskite layers fabricated through intramolecular exchange, *Science*, 2015, **348**, 1234–1237.

8 W. S. Yang, B.-W. Park, E. H. Jung, N. J. Jeon, Y. C. Kim, D. U. Lee, S. S. Shin, J. Seo, E. K. Kim, J. H. Noh and S. I. Seok, Iodide management in formamidinium-lead-halide-based perovskite layers for efficient solar cells, *Science*, 2017, **356**, 1376–1379.

9 National Renewable Energy Laboratory, *Best Research-Cell Efficiency chart*, 2020, https://www.nrel.gov/pv/cell-efficiency.html.

10 H. Gao, C. Bao, F. Li, T. Yu, J. Yang, W. Zhu, X. Zhou, D. Fu and Z. Zou, Nucleation and Crystal Growth of Organic−Inorganic Lead Halide Perovskites under Different Relative Humidity, *ACS Appl. Mater. Interfaces*, 2015, **7**, 9110–9117.

11 Y. Zhang, S. G. Kim, D. Lee, H. Shin and N. G. Park, Bifacial stamping for high efficiency perovskite solar cells, *Energy Environ. Sci.*, 2019, **12**, 308–321.

12 J. K. Nam, S. U. Chai, W. Cha, Y. J. Choi, W. Kim, M. S. Jung, J. Kwon, D. Kim and J. H. Park, Potassium Incorporation for Enhanced Performance and Stability of Fully Inorganic Cesium Lead Halide Perovskite Solar Cells, *Nano Lett.*, 2017, **17**, 2028–2033.

13 Q. Chen, H. Zhou, Z. Hong, S. Luo, H. Duan, H. H. Wang, Y. Liu, G. Li and Y. Yang, Planar Heterojunction Perovskite Solar Cells *via* Vapor-Assisted Solution Process, *J. Am. Chem. Soc.*, 2014, **136**(2), 622–625.

14 J. Burschka, N. Pellet, S. J. Moon, R. Humphry-Baker, P. Gao, M. K. Nazeeruddin and M. Grätzel, Sequential deposition as

a route to high-performance perovskite-sensitized solar cells, *Nature*, 2013, **499**(7458), 316–3199.

15 L. Chen, X. Xie, Z. Liu and E. C. Lee, A transparent poly(3,4-ethylenedioxylenethiophene):poly(styrene sulfonate) cathode for low temperature processed, metal-oxide free perovskite solar cells, *J. Mater. Chem. A*, 2017, **5**, 6974–6980.

16 M. Saliba, T. Matsui, K. Domanski, J. Y. Seo, A. Ummadisingu, S. M. Zakeeruddin, J. P. Correa-Baena, W. R. Tress, A. Abate, A. Hagfeldt and M. Grätzel, Incorporation of rubidium cations into perovskite solar cells improves photovoltaic performance, *Science*, 2016, **354**, 206–209.

17 H. Kim, J. Y. Seo and N.-G. Park, Material and Device Stability in Perovskite Solar Cells, *ChemSusChem*, 2016, **9**, 2528–2540.

18 S. Yang, W. Fu, Z. Zhang, H. Chen and C.-Z. Li, Recent advances in perovskite solar cells: efficiency, stability and lead-free perovskite, *J. Mater. Chem. A*, 2017, **5**, 11462–11482.

19 K. Chondroudis and D. B. Mitzi, Electroluminescence from an Organic−Inorganic Perovskite Incorporating a Quaterthiophene Dye within Lead Halide Perovskite Layers, *Chem. Mater.*, 1999, **11**, 3028–3030.

20 E. R. Dohner, A. Jaffe, L. R. Bradshaw and H. I. Karunadasa, Intrinsic White-Light Emission from Layered Hybrid Perovskites, *J. Am. Chem. Soc.*, 2014, **136**, 13154–13157.

21 C. R. Kagan, D. B. Mitzi and C. D. Dimitrakopoulos, Organic–Inorganic Hybrid Materials as Semiconducting Channels in Thin-Film Field-Effect Transistors, *Science*, 1999, **286**, 945–947.

22 Z. Tan, Y. Wu, H. Hong, J. Yin, J. Zhang, L. Lin, M. Wang, X. Sun, L. Sun, Y. Huang, K. Liu, Z. Liu and H. Peng, Two-Dimensional $(C_4H_9NH_3)_2PbBr_4$ Perovskite Crystals for High-Performance Photodetector, *J. Am. Chem. Soc.*, 2016, **138**, 16612–16615.

23 X. Zhang, G. Wu, S. Yang, W. Fu, Z. Zhang, C. Chen, W. Liu, J. Yan, W. Yang and H. Chen, Vertically Oriented 2D Layered Perovskite Solar Cells with Enhanced Efficiency and Good Stability, *Small*, 2017, **13**, 1700611.

24 F. Zhang, D. Kim and K. Zhu, 3D/2D Multidimensional perovskites: balance of high performance and stability for perovskite solar cells, *Curr. Opin. Electrochem.*, 2018, **11**, 105–113.

25 P. Chen, Y. Bai, M. Q. Lyu, J. H. Yun, M. M. Hao and L. Z. Wang, Progress and Perspective in Low-Dimensional Metal Halide Perovskites for Optoelectronic Applications, *Sol. RRL*, 2018, **2**, 1700186.

26 S. Shahiduzzaman, K. Yamamoto, Y. Furumoto, K. Yonezawa, K. Hamada, K. Kosuke, K. Ninomiya, M. Makoto Karakawa, T. Kuwabara, K. Takahashi, K. Takahashi and T. Taima, Viscosity effect of ionic liquid-assisted controlled growth of $CH_3NH_3PbI_3$ nanoparticle-based planar perovskite solar cells, *Org. Electron.*, 2017, **48**, 147–153.

27 Q. He, M. Worku, L. Xu, C. Zhou, S. Lteif, J. Schlenoff and B. Ma, Surface Passivation of Perovskite Thin Films by Phosphonium Halides for Efficient and Stable Solar Cells, *J. Mater. Chem. A*, 2020, **8**, 2039–2046.

28 D. F. Garcia-Gutierrez, D. I. Garcia-Gutierrez, D. González-Quijano, I. A. Abarca-Villarreal, S. F. Galindo-Garza and E. M. Sanchez, Improving ambient stability of BiI_3-based perovskites using different phosphoniums as the organic cation, *MRS Commun.*, 2018, **8**, 878–884.

29 X. Li., M. I. Dar, C. Yi, J. Luo, M. Tschumi, S. M. Zakeeruddin, M. K. Nazeeruddin, H. Han and M. Grätzel, Improved performance and stability of perovskite solar cells by crystal crosslinking with alkylphosphonic acid ω-ammonium chlorides, *Nat. Chem.*, 2015, **7**(9), 703–711.

30 N. Karodia, S. Guise, C. Newlands and J. Andersen, Clean catalysis with ionic solvents—phosphonium tosylates for hydroformylation, *Chem. Commun.*, 1998, **21**, 2341–2342.

31 A. A. Sutanto, S. Lan, C.-F. Cheng, S. B. Mane, H.-P. Wu, M. Leonardus, M. Y. Xie, S. C. Yeh, C. W. Tseng, C. T. Chen, E. W.-G. Diau and C. H. Hung, Solvent-assisted crystallization *via* a delayed-annealing approach for highly efficient hybrid mesoscopic/planar perovskite solar cells, *Sol. Energy Mater. Sol. Cells*, 2017, **172**, 270–276.

32 J. J. Kiddle, Microwave irradiation in organophosphorus chemistry. III. Moderate scale synthesis of reagents for olefin formation, *Synth. Commun.*, 2001, **31**, 3377–3382.

33 V. P. Balema, J. W. Wiench, M. Pruski and V. K. Pecharsky, Solvent-free mechanochemical synthesis of phosphonium salts, *Chem. Commun.*, 2002, 724–725.

34 V. V. Namboodiri and R. S. Varma, Solvent-Free Sonochemical Preparation of Ionic Liquids, *Org. Lett.*, 2002, **4**, 3161–3163.

35 J. Qing, H.-T. Chandran, Y.-H. Cheng, X.-K. Liu, H.-W. Li, S.-W. Tsang, M. F. Lo and C. S. Lee, Chlorine Incorporation for Enhanced Performance of Planar Perovskite Solar Cell Based on Lead Acetate Precursor, *ACS Appl. Mater. Interfaces*, 2015, **7**, 23110–23116.

36 Y. Liu, Z. Liu and E. C. Lee, Dimethyl-sulfoxide-assisted improvement in the crystallization of lead-acetate-based perovskites for high-performance solar cells, *J. Mater. Chem. C*, 2018, **6**, 6705–6713.

37 H. Wei, J. Xiao, Y. Yang, S. Lv, J. Shi, X. Xu, J. Dong, Y. Luo, D. Li and Q. Meng, Free-standing flexible carbon electrode for highly efficient hole-conductor-free perovskite solar cells, *Carbon*, 2015, **93**, 861–868.

38 M. Yuan, L. N. Quan, R. Comin, G. Walters, R. Sabatini, O. Voznyy, S. Hoogland, Y. Zhao, E. M. Beauregard, P. Kanjanaboos, Z. Lu, D. H. Kim and E. H. Sargent, Perovskite energy funnels for efficient light-emitting diodes, *Nat. Nanotechnol.*, 2016, **11**, 872–877.

39 N. Wang, L. Cheng, R. Ge, S. Zhang, Y. Miao, W. Zou, C. Yi, Y. Sun, Y. Cao, R. Yang, Y. Wei, Q. Guo, Y. Ke, M. Yu, Y. Jin, Y. Liu, Q. Ding, D. Di, L. Yang, G. Xing, H. Tian, C. Jin, F. Gao, R. H. Friend, J. Wang and W. Huang, Perovskite light-emitting diodes based on solution-processed self-organized multiple quantum wells, *Nat. Photonics*, 2016, **10**, 699–704.

40 D. H. Cao, C. C. Stoumpos, O. K. Farha, J. T. Hupp and M. G. Kanatzidis, 2D homologous perovskites as light-absorbing materials for solar cell applications, *J. Am. Chem. Soc.*, 2015, **137**, 7843–7850.

41 W. Ke, L. Mao, C. C. Stoumpos, J. Hoffman, I. Spanopoulos, A. D. Mohite and M. G. Kanatzidis, Compositional and Solvent Engineering in Dion–Jacobson 2D Perovskites Boosts Solar Cell Efficiency and Stability, *Adv. Energy Mater.*, 2019, **9**, 1803384.

42 J. Yang, B. D. Siempelkamp, D. Liu and T. L. Kelly, Investigation of $CH_3NH_3PbI_3$ Degradation Rates and Mechanisms in Controlled Humidity Environments Using *in situ* Techniques, *ACS Nano*, 2015, **9**, 1955–1963.

43 A. M. A. Leguy, Y. Hu, Q. M. Campoy, M. Alonso, O. J. Weber, P. Azarhoosh, M. Schilfgaarde, M. T. Weller, T. Bein, J. Nelson, P. Docampo and P. R. F. Barnes, Reversible Hydration of $CH_3NH_3PbI_3$ in Films, Single Crystals, and Solar Cells, *Chem. Mater.*, 2015, **27**, 3397–3407.

44 A. Mahapatra, D. Prochowicz, M. Mahdi, S. Trivedi, P. Kumara and P. Yadav, A review of aspects of additive engineering in perovskite solar cells, *J. Mater. Chem. A*, 2020, **8**, 27–54.

45 S. Jin, Y. Wei, B. Rong, Y. Fang, Y. Zhao, Q. Guo, Y. Huang, L. Fan and J. Wu, Improving perovskite solar cells photovoltaic performance using tetrabutylammonium salt as additive, *J. Power Sources*, 2020, **2450**, 227623–227630.

46 X. Huang, H. Guo, K. Wang and X. Liu, Ionic liquid induced surface trap-state passivation for efficient perovskite hybrid solar cells, *Org. Electron.*, 2017, **41**, 42–48.

47 w. Zhang, X. Lei, J. Liu, J. Dong, X. Yan, W. Gao, H. Dong, C. Ran and Z. Wu, Efficient Charge Collection Promoted by Interface Passivation Using Amino Acid Toward High Performance Perovskite Solar Cells, *Phys. Status Solidi RRL*, 2019, **13**, 1800505–1800510.

48 Y. Liao, H. Liu, W. Zhou, D. Yang, Y. Shang, Z. Shi, B. Li, X. Jiang, L. Zhang, L. N. Quan, R. Quintero-Bermudez, B. R. Sutherland, Q. Mi, E. H. Sargent and Z. Ning, Highly Oriented Low-Dimensional Tin Halide Perovskites with Enhanced Stability and Photovoltaic Performance, *J. Am. Chem. Soc.*, 2017, **139**, 6693–6699.

49 T. Y. Wen, S. Yang, P. F. Liu, L. J. Tang, H. W. Qiao, X. Chen, X. H. Yang, Y. Hou and H. G. Yang, Surface Electronic Modification of Perovskite Thin Film with Water-Resistant Electron Delocalized Molecules for Stable and Efficient Photovoltaic, *Adv. Energy Mater.*, 2018, **8**, 1703143–1703149.

50 N. K. Noel, A. Abate, S. D. Stranks, E. S. Parrott, V. M. Burlakov, A. Goriely and H. J. Snaith, Enhanced Photoluminescence and Solar Cell Performance *via* Lewis Base Passivation of Organic–Inorganic Lead Halide Perovskites, *ACS Nano*, 2014, **8**, 9815–9821.